



Early Detection of Chikungunya Virus Utilizing the Surface Plasmon Resonance Comprising a Silver-Silicon-PtSe₂ Multilayer Structure

Thangjam Iboyaima Singh¹ · Pawan Singh¹ · Bhisma Karki^{2,3,4}

Received: 2 March 2023 / Accepted: 3 April 2023 / Published online: 19 April 2023
© The Author(s), under exclusive licence to Springer Science+Business Media, LLC, part of Springer Nature 2023

Abstract

The sensing performance parameters of the SPR sensors are sensitivity, detection accuracy, the figure of merit (FOM), and full-width half maximum (FWHM), and it has been discussed with refractive indexes of analyte 1.33, 1.35, 1.38, and 1.39. In this, we proposed a multilayer structure comprising nanofilms of Ag, Silicon, and PtSe₂ for the early diagnosis of chikungunya virus. The suggested sensor structure consists of a BK7 (borosilicate crown) coupling prism over which the nanofilm of silver metal is present. The layer thicknesses and the number of silicon and PtSe₂ sheets are optimized for high performance. At the operating wavelength of 633 nm, a Kretschmann-based SPR sensor has been proposed, which gives the highest sensitivity of 287.3 Deg/RIU. The principle of attenuated total reflection has been employed for the performance analysis of the sensor.

Keywords Chikungunya virus · SPR · Sensitivity · Kretschmann configuration · Silicon · Platinum diselenide

Introduction

Chikungunya is an RNA virus belonging to the *Togaviridae* family's alphavirus genus. Chikungunya is a Kima-konde word that means “to twist.” In 1952, CHIKV was found for the first time in the United Republic of Tanzania. It was later found in other places in Africa and Asia. In 1967, Thailand and India were the first countries to report urban outbreaks. Since 2004, there have been more and bigger CHIKV outbreaks. CHIKV has been found in over 110 countries in Asia, Africa, Europe, and the Americas. The reverse transcriptase-polymerase chain reaction may be used to identify the Chikungunya virus in early blood samples (RT-PCR). Other assays can reveal chikungunya immune response. After a week of infection, these tests look for viral

antibodies. Antibody levels are apparent within a week after sickness starts and can last 2 months [1].

During 2005–2006, there were more than two hundred thousand reported chikungunya cases on Réunion Island in the Indian Ocean, with a case-fatality rate of 1/1000. In 2006, India experienced a major chikungunya outbreak, with more than one million cases reported in 151 districts and ten states [2]. In Ahmedabad, with a population of roughly four million, there were approximately 60,000 suspected cases of chikungunya. During this outbreak, the attack rate (the percentage of a population affected by the disease) reached 45% in some areas. To determine the impact of the pandemic on Ahmedabad, death rates in 2006 were compared to the average number of deaths in the same months during the preceding four years. The analysis found 2944 additional fatalities during the chikungunya pandemic (August–November 2006). Chikungunya has been present in India since 1973, when the attack rate was 37.5%. However, no deaths directly related to chikungunya have been documented in India [3], unlike the Réunion Island outbreak. The most common vectors for transmitting the disease in these areas were *Aedes albopictus* on Réunion Island and *Aedes aegypti* in India.

Surface plasmon resonance (SPR) sensors are particular, accurate, and quantifiable, and do not require molecular labeling (label-free). Any target, from tiny molecules like methane and carbon dioxide to microorganisms, may be identified. SPR is an affinity/immunoassay specialist. It

✉ Bhisma Karki
magnum.photon@gmail.com

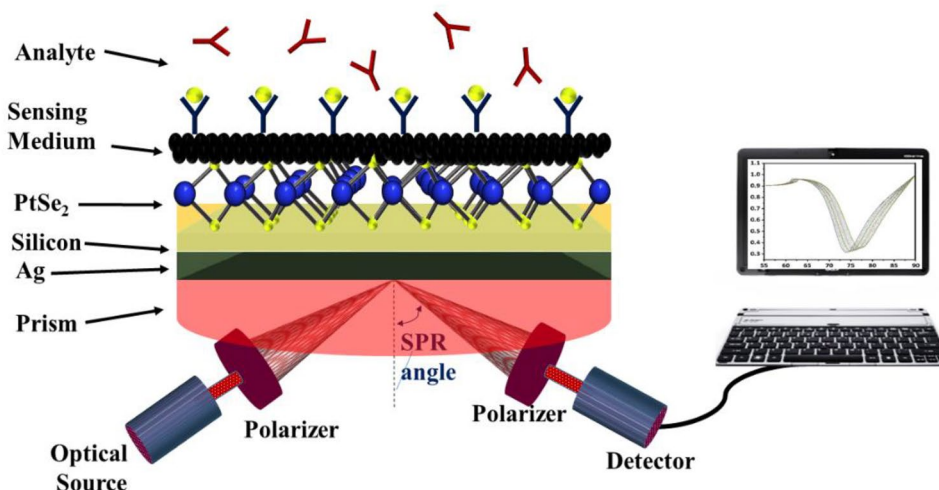
¹ Department of Physics, Himalayiya University, Doiwala, Dehradun, Uttarakhand 248140, India

² Department of Physics, Tri-Chandra Multiple Campus, Tribhuvan University, Kathmandu 44600, Nepal

³ National Research Council Nepal, New Baneshwor-10, Kathmandu 44600, Nepal

⁴ Department of Physics and Research Centre, Tuljaram Chaturchand College Baramati, Pune 413102, India

Fig. 1 Schematic diagram of the proposed sensor



employs a planar waveguide to create an evanescent wave, where light is internally reflected. Gold metallization of the waveguide surface interacts with electromagnetic waves at the metal–liquid contact. Light coupling into the metal layer and reduction of reflection intensity are proportional to refractive index variances in the fluid near the metal surface. Continuous monitoring of a refractive index change owing to macromolecular surface binding (e.g., an immunoreaction) is possible. It thus allows immediate, real-time tracking of surface affinity responses. SPR biosensors can detect even minute shifts in the refractive index in areas where biomolecules bind with receptors mounted on an optical transducer’s surface [4, 5]. Prism-based SPR sensors are popular nowadays. A photonic crystal-based biosensor has also been proposed for chikungunya detection. The maximum sensitivity 3.43×10^3 nm/RIU has been reported here [6]. The application of SPR-based biosensors for the detection of pathogens in water has been examined by several researchers [7–9].

Platinum diselenide (PtSe₂) is a new transition metal dichalcogenide (TMD) family member with exceptional electrical and optical properties. For instance, high carrier mobility electrical qualities have been used in solar cells, and other properties, such as a variable band gap and strong optical absorption, have also been observed [10–13]. 2D TMDs have the potential to be used in biosensor technology

because of their outstanding biocompatibility [12, 14] with the analyte.

This work developed a new SPR sensor structure using a PtSe₂ heterostructure together with silicon/ Ag/ and a comprehensive examination of the traditional structure was performed. For sensor analysis, angular interrogation, a method based on attenuated total reflection (ATR), is considered here. The sensitivity (S), detection accuracy (DA), the figure of merit (FOM), quality factor (QF), and other features of the sensor are investigated here in this work and are discussed in the following sections.

Structure of Proposed SPR Sensor

A schematic model of a biosensor based on the Kretschmann configuration is shown in Fig. 1. This proposed SPR biosensor is a five-layer system consisting of a BK7 prism, a silver (Ag) layer, a silicon (Si) layer, and a platinum diselenide (PtSe₂) monolayer and sensing medium. P-polarized light with an operating wavelength of 633 nm is directed at the prism/metal interface beyond the critical angle. A photodetector can be used to identify and examine the reflected light.

The proposed SPR design parameters are summarized in Table 1.

Table 1 Layer materials with thicknesses and refractive index for proposed work

Layer	Material	Thickness (nm)	Refractive index at (633 nm)	Ref.
First	Prism (BK7)	-	1.515	[15]
Second	Silver (Ag)	55	$0.0563 + i*4.276$	[16]
Third	Silicon	0.33	3.9160	[17]
Fourth	Platinum di selenide (PtSe ₂)	0.34	$2.8528 + i* 1.1129$	[18]

The subsequent sections of the document are arranged as follows: Section “Methodology and Considerations” contains theoretical modeling considerations, and mathematical formulas needed to analyze sensor performance. Section “Results and Discussion” of this work describes the results and analysis, while Section “Conclusion” includes the conclusion and discussions.

Methodology and Considerations

At the interface of the metal-dielectric boundary, electrons are stimulated and form a cloud of electrons, known as surface plasmon, that are oscillating at a certain frequency. Attenuated total reflection (ATR) occurs when light travels through a prism with a thin metal film (typically Au or Ag) at angles greater than the critical angle (AIR). Under AIR circumstances, the photon permeates the metal and passes its energy to oscillating electrons, causing SPR. This happens when the incidence wave vector (K_i) matches the surface plasmon wave vector (K_p) [19]. Light alone cannot excite the plasmon. Therefore, it gets extra acceleration from the prism to achieve resonance. When photon energy is transmitted to oscillating electrons, resonance and a drop in reflected light intensity result. The resonance angle or SPR angle is the largest dip in intensity. On the other side, an evanescent wave will arise and disintegrate exponentially. Evanescent waves detect changes in metal’s refractive index (within 200 nm). Binding of the analyte with the sensing medium causes a change in the refractive index on the other side, affecting electron oscillation. This change in plasmon speed modifies the incident light vector needed for SPR, shifting the resonance angle. Monitoring SPR dip angle over time provides a sensor graph of reaction versus time, visualizing binding. Finally, it is worth noting that SPR devices have emerged as promising contenders for the fast detection of chemical and biological components in domains like environmental monitoring. Its appealing characteristics and functionalities suggest it might be important in fostering public health and safeguarding environments.

The suggested biosensor is envisaged to comprise five layers consisting Fig. 1. In this, the sensing medium blood components such as platelets and plasmas must be utilized for the identification of the chikungunya virus. The glass prism refractive index was found based on the equation [17, 20] as follows:

$$RI_{prism} = (1 + \frac{A_1 \lambda^2}{\lambda^2 - B_1} + \frac{A_2 \lambda^2}{\lambda^2 - B_2} + \frac{A_3 \lambda^2}{\lambda^2 - B_3})^{1/2} \tag{1}$$

where A_i and B_i are the coefficients which are given as $A_1 = 0.971247817$, $A_2 = 0.216901417$, $A_3 = 0.904651666$, $B_1 = 0.00472301995$, $B_2 = 0.0153575612$, and $B_3 = 168.68133$. Here, “ λ ” is the wavelength of the incident wave (in nm). The wavelength-dependent refractive index of the Silver layer is expressed by the Drude-Lorentz model [21].

$$RI_{silver} = (1 - \frac{\lambda_{cw} \lambda^2}{\lambda_{pw}^2 (\lambda_{cw} + i\lambda)})^{1/2} \tag{2}$$

where λ_{cw} , collision wavelength = 1.7614×10^{-5} m, and λ_{pw} , plasma wavelength = 1.4541×10^{-7} m of Ag. The graphene refractive index can be calculated by [19, 22]:

$$RI_g = (3 + \lambda \frac{K}{3} i)^{1/2} \tag{3}$$

where K is a constant equal to $5.446 \mu\text{m}^{-1}$. The refractive index of Silicon was given by the following relation [20, 23]:

$$RI_s = 1 + \frac{10.668493 \lambda^2}{\lambda^2 - (0.301516485)^2} + \frac{0.00304347 \lambda^2}{\lambda^2 - (1.13475115)^2} + \frac{1.54133408 \lambda^2}{\lambda^2 - (1104.0)^2} \tag{4}$$

For the excitation of SP waves, the SP and TM incident light propagation constants must be the same, which may be expressed mathematically as.

$$(\omega/c)(\epsilon_{prism})^{1/2} \sin \alpha_{in} = (\omega/c)(\epsilon_{Ag} \epsilon_d / (\epsilon_{Ag} + \epsilon_d))^{1/2} \tag{5}$$

where ϵ_{prism} , ω , ϵ_{Ag} , α_{in} , and ϵ_d are the permittivity of the prism, the frequency of the incident wave, the permittivity of the metal, the angle of incidence, and the dielectric permittivity, respectively. Along the z -axis, the various levels of the SPR structure are stacked. The dielectric constant and thickness of each layer are ϵ_K and d_K respectively. The tangential field components at the first interface ($z=0$) may be expressed mathematically in terms of those at the final interface ($z=z_{N-1}$) as

$$\begin{bmatrix} EF_1 \\ MF_1 \end{bmatrix} = FL_T \begin{bmatrix} EF_{N-1} \\ MF_{N-1} \end{bmatrix} \tag{6}$$

where EF_1 and EF_{N-1} are the first and the last boundaries of tangential electric fields, respectively. MF_1 and MF_{N-1} are the first and the last boundaries of tangential magnetic fields, respectively. FL_T is the transfer matrix that connects the first to the last boundary field. For the j^{th} layer, the characteristic matrix (C_j) is expressed by [24]:

$$C_j = \begin{bmatrix} \cos \phi_j & -i \frac{\sin \phi_j}{P_j} \\ -i P_j \sin \phi_j & \cos \phi_j \end{bmatrix} \tag{7}$$

ϕ_j is the phase shift of the light wave due to propagation through the j^{th} layer. Its value is

$$\phi_j = \frac{2\pi}{\lambda} d_j (\epsilon_j - (n_1 \sin \alpha_1)^2)^{1/2} \tag{8}$$

where n_1 and α_1 are the refractive index and the incident angle of the prism. For TM waves, P_j is given by:

$$P_j = (\epsilon_j - (n_1 \sin \alpha_1)^2)^{1/2} / \epsilon_j \tag{9}$$

The system transfer matrix (C_T) is given as the product of the individual matrices of the layers.

$$C_T = C_{Ag}C_S C_G = \begin{bmatrix} C_{11} & C_{12} \\ C_{21} & C_{22} \end{bmatrix} \quad (10)$$

The reflection coefficient (K_r) of the structure is given in terms of the system transfer matrix C_{ij} as [25]

$$K_r = \frac{(C_{11} + C_{11}P_N)P_1 - (C_{21} + C_{22}P_N)}{(C_{11} + C_{11}P_N)P_1 + (C_{21} + C_{22}P_N)} \quad (11)$$

The reflection intensity (R) of the proposed system is expressed as [26]

$$R = r.r^* = |r|^2 \quad (12)$$

Sensor sensing capability of biosensor computed by this parameter sensitivity (S) [27]. Mathematically sensitivity is expressed as $S = \frac{\Delta\theta_{SPR}}{\delta n_s}$; its unit is DegRIU⁻¹. The notations $\Delta\theta_{SPR}$ and δn_s signify the variation in SPR angle at resonance and change in the RI of the sensing medium.

FWHM is the SPR curve width at half of the reflectance, and expressed as: $FWHM = \theta_b - \theta_a$, unit is in Deg [28]. The detection accuracy (DA) parameter calculates the sensor's exactness. Numerically expressed by [29]: $DA = FWHM^{-1}$

(expressed in Deg⁻¹). Another parameter that calculates the quality of the sensor is the figure of merit (FOM) or quality factor (Q). Mathematically expressed by [30]: $FOM = S.DA$, its unit is RIU⁻¹.

Results and Discussion

This section of the manuscript shows the results and discussions of the proposed simulation study. Figure 2 gives the reflectance spectra for the different scenarios of layers of silicon (Si) and PtSe₂ (Pt). The computed parameters such as SPR angle (θ), minimum reflectance (R_{min}), sensitivity, FWHM, DA, and FOM for (a) [Si=0, Pt=0], (b) [Si=0, Pt=1], (c) [Si=1, Pt=0], and (d) [Si=1, Pt=1] are given in Table 2.

For the conventional SPR setup, i.e., Prism/Ag/Sensing Medium (Si=0, Pt=0), the angular sensitivity was computed to be 169.1 deg/RIU maximum. After that, inserting a mono layer of PtSe₂ with no silicon layer (Si=0, Pt=1) in between the sensing medium and Ag layer, the highest sensitivity enhanced to 174.4 deg/RIU. Furthermore, for Si=1, and Pt=0, the maximum value of angular sensitivity varies to 239.7 deg/RIU. For single silicon and single PtSe₂ layer (Si=1, Pt=1) (Fig. 2d), the maximum computed value

Fig. 2 Reflectance plots for different incidence angles for **a** Si=0, Pt=0; **b** Si=0, Pt=1; **c** Si=1, Pt=0; and **d** Si=1, Pt=1

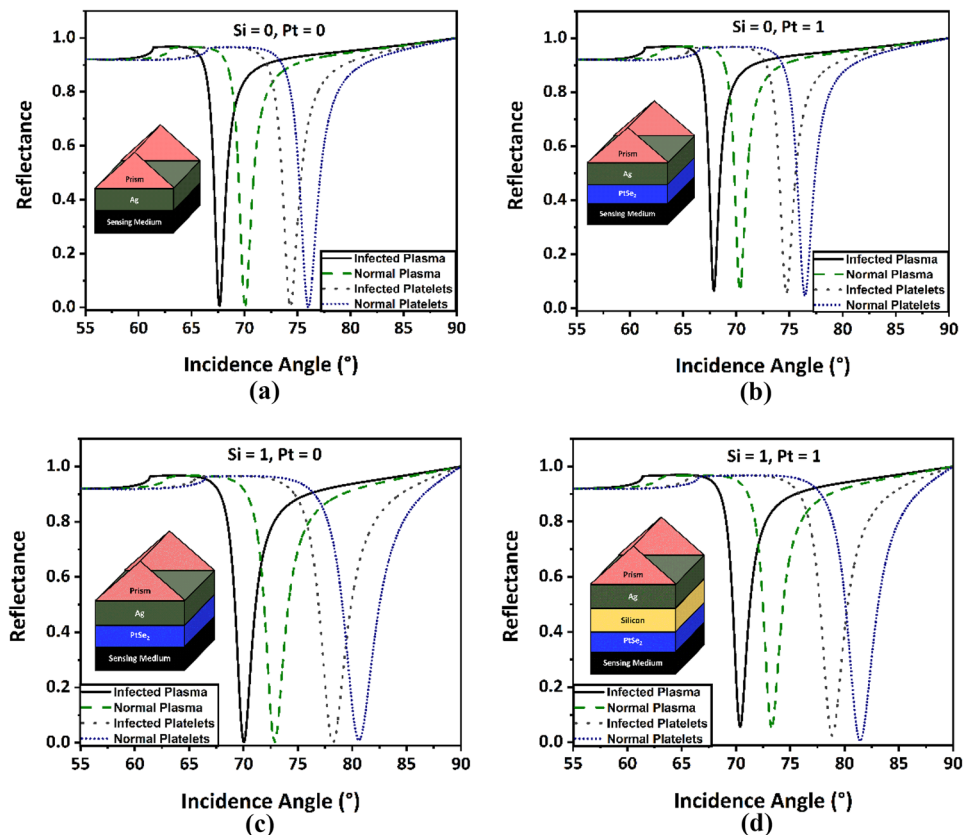


Table 2 Performance parameters calculated for Silicon and PtSe₂ layers

Si = 0, Pt = 0						
RI	Θ	R_{min}	S	FWHM	DA	FOM
1.33 (infected plasma)	67.64	0.00589	-	1.28	-	-
1.35 (normal plasma)	70.055	0.00549	120.75	1.466	0.682	82.36
1.38 (infected platelets)	74.323	0.00257	142.26	1.865	0.536	76.28
1.39 (normal platelets)	76.014	0.00096	169.1	2.053	0.487	82.36
Si = 0, Pt = 1						
RI	Θ	R_{min}	S	FWHM	DA	FOM
1.33 (infected plasma)	67.889	0.06541	-	1.066	-	-
1.35 (normal plasma)	70.343	0.06547	122.70	1.219	0.820	100.65
1.38 (infected platelets)	74.705	0.05608	145.40	1.555	0.643	93.50
1.39 (normal platelets)	76.449	0.04755	174.40	1.72	0.581	101.39
Si = 1, Pt = 0						
RI	Θ	R_{min}	S	FWHM	DA	FOM
1.33 (infected plasma)	70.033	0.00287	-	1.908	-	-
1.35 (normal plasma)	72.86	0.00171	141.35	2.228	0.448	63.44
1.38 (infected platelets)	78.224	0.000888	178.80	2.993	0.334	59.73
1.39 (normal platelets)	80.621	0.00953	239.70	3.42	0.292	70.08
Si = 1, Pt = 1						
RI	Θ	R_{min}	S	FWHM	DA	FOM
1.33 (infected plasma)	70.382	0.05756	-	1.59	-	-
1.35 (normal plasma)	73.281	0.05287	144.95	1.86	0.537	77.93
1.38 (infected platelets)	78.859	0.02451	185.93	2.56	0.390	72.65
1.39 (normal platelets)	81.432	0.00584	257.30	3.01	0.332	85.45

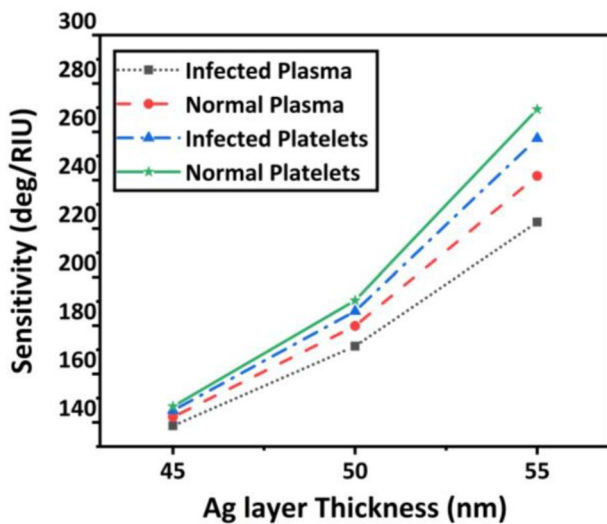


Fig. 3 Variation in angular sensitivity for different Ag thicknesses

for angular sensitivity attained is 257.3 deg/RIU. So, these results show that after the addition of both Si and Pt layers over the conventional design, the sensitivity is enhanced due to maximum optical light absorption with the presence of silicon and PtSe₂.

Table 3 Sensitivity calculations for the number of silicon layers and PtSe₂ layers for platelets and plasma cases

No. of silicon layers	1	2	3
Sensitivity (deg/RIU) [platelets]	144.95	185.93	257.3
sensitivity (deg/riu) [plasma]	149.35	205.33	287.3
No. of PtSe₂ layers	1	2	3
Sensitivity (deg/RIU) [platelets]	144.95	185.93	257.3
Sensitivity (deg/RIU) [plasma]	148.6	194.16	279.9

Fig. 4 Sensitivity as a function of the number of **a** silicon layers and **b** PtSe₂ layers

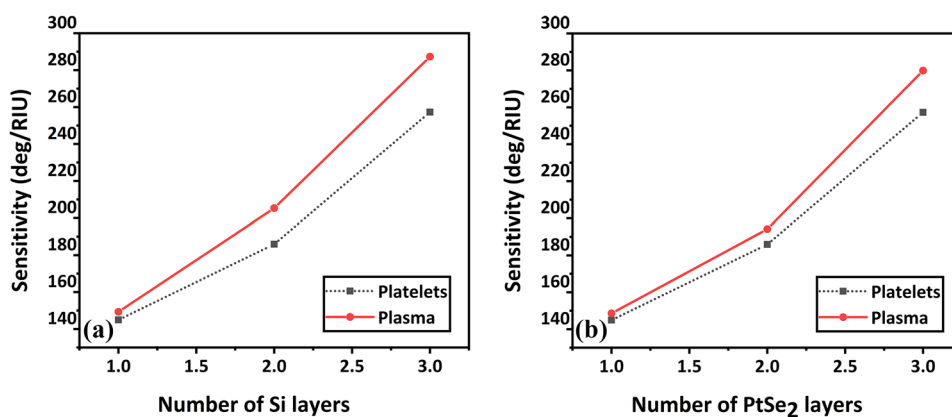


Table 4 Comparison of sensitivity parameter values of current SPR work with latest SPR works

Reference	Structures (prime layers)	Targeted application	Sensitivity
[31]	Ag-InP-BP	Formalin detection	250.2 deg/RIU
[32]	Au-BP-Au-Graphene	Chemical sensing	218 deg/RIU
[33]	Au-SnSe-Au-Graphene	Biomolecular analytes	214 deg/RIU
[34]	Ag-BaTiO ₃ -Ag-Graphene	Biomedical sensing	280 deg/RIU
[35]	Ag-Si-Graphene	Chikungunya virus	393 to 160 deg/RIU
Current SPR work	Ag-Si-PtSe ₂	Chikungunya virus	287.3 deg/RIU

Silver Layer Optimization

The angular sensitivity gets calculated for three different layer thicknesses of Ag (45 nm, 50 nm, and 55 nm). The RI considered here is 1.33 (infected plasma), 1.35 (normal plasma), 1.38 (infected plasma), and 1.39 (normal plasma). The computed sensitivity value maximum for 55 nm of thickness attained is 269.3 deg/RIU for normal platelets. Therefore, the optimized thickness of the Ag layer 55nm has been considered (Fig. 3).

The values of angular sensitivity by altering the number of silicon and PtSe₂ layers have been calculated (Table 3). As the number of silicon and PtSe₂ layers increases, the absorbance of the optical signal has been increased, and the dip on the resonance is also increased, ultimately increasing the sensitivity of the sensor. The number of silicon and PtSe₂ has been increased by more than three layers; the sensitivity decreases. In the three layers of silicon and PtSe₂, we attained the maximum sensitivity of 287.3 and 279.9 in deg/RIU for both plasma cases. Figure 4a implies that the sensitivity can be further enhanced by increasing the silicon layers (1 to 3) because of the change in the reflectance dip to a greater incidence angle. We also observed that the same trend is observed by enhancing the PtSe₂ layers (PtSe₂ = 1 to 3) also with a single silicon layer (Fig. 4b).

Furthermore, the comparison with other SPR-based sensors reported earlier is shown here. Table 4 shows that the proposed study's sensitivity parameters are more comparable to other studies in the reported literature.

Conclusion

An RNA-based virus called the chikungunya virus infects mosquitoes which bite humans. The most typical signs of this infection include fever, joint swelling, discomfort, and muscle soreness. With the advantages like label-free sensing, real-time detection, and low cost, SPR sensors are popular sensing techniques. Here we proposed a layered heterostructure architecture of SPR sensors consisting of BK7 prism (coupling)/Ag (metal)/silicon/PtSe₂(TMD)/sensing medium (analyte) for the early detection of chikungunya virus. The analysis of the sensor has been carried out using TMM. The thickness of the Ag layer has been optimized. The optimum thickness of Ag layer 55 nm has been taken. Optimizing the layers has been done to enhance the sensor's sensitivity. For three silicon layers and one PtSe₂ layer, the highest sensitivity has been calculated as 287.3 deg/RIU for the case of plasma. The four types of blood cells have been analyzed using the proposed SPR sensor.

Acknowledgements We would like to thank all the members of the Department of Physics, Tri-Chandra Multiple Campus, Kathmandu-44600, Himalayiya University, Doiwala, Dehradun, Uttarakhand-248140, India, Department of Physics and Research Centre, Tuljaram Chaturchand College Baramati, Pune—413102, India, and National Research Council Nepal for their kind support during this work.

Author Contribution TIS provided statistical analysis for the results. He provided the theoretical background to SPR biosensors. PS provided the theoretical background to biosensing and importance of optical biosensing. BK formulated the problem statement wherein giving the theoretical background for SPR biosensor. He also helped in drafting the manuscript.

Declarations

Ethics Approval Not applicable. The work presented in this manuscript is mathematical modeling only for the proposed biosensor. No experiment was performed on the human body and/or living organism/animal. So, an ethical approval from an ethical committee is not required.

Consent to Participate All the authors are willing to participate in the work presented in this manuscript. On the behalf of all authors, the communicating author is authorized to give their consent.

Consent for Publication All the authors have given their consent to publish this work.

Conflict of Interest The authors declare no competing interests.

References

- Mavalankar D, Shastri P, Bandyopadhyay T, Parmar J, Ramani KV (2008) Increased mortality rate associated with chikungunya epidemic, Ahmedabad, India. *Emerg Infect Dis* 14(3):412–415. <https://doi.org/10.3201/eid1403.070720>
- Shi J et al (2017) Extensive evolution analysis of the global chikungunya virus strains revealed the origination of CHIKV epidemics in Pakistan in 2016. *Virology* 520(6):520–532. <https://doi.org/10.1007/s12250-017-4077-5>
- Byahatti SM, Dandagi GL (2010) Chikungunya- an update. *J Clin Diagn Res* 4(6):3594–3598
- Poltronieri P, Mezzolla V, Primiceri E, Maruccio G (2014) Biosensors for the detection of food pathogens. *Foods* 3(3):511–526. <https://doi.org/10.3390/foods3030511>
- Patching SG (2014) Surface plasmon resonance spectroscopy for characterisation of membrane protein-ligand interactions and its potential for drug discovery. *Biochim. Biophys. Acta - Biomembr.* 1838(1 Part A):43–55. <https://doi.org/10.1016/j.bbame.2013.04.028>
- Sharma S, Kumar A, Singh KS, Tyagi HK (2021) 2D photonic crystal based biosensor for the detection of chikungunya virus. *Optik (Stuttg)* 237:166575. <https://doi.org/10.1016/j.ijleo.2021.166575>
- Yakes BJ et al (2013) Surface plasmon resonance biosensor for detection of feline calicivirus, a surrogate for norovirus. *Int J Food Microbiol* 162(2):152–158. <https://doi.org/10.1016/j.ijfoodmicro.2013.01.011>
- Masdor NA, Altintas Z, Tothill IE (2017) Surface plasmon resonance immunosensor for the detection of *Campylobacter jejuni*. *Chemosensors* 5(2):1–15. <https://doi.org/10.3390/chemosensors5020016>
- Wang Y, Knoll W, Dostalek J (2012) Bacterial pathogen surface plasmon resonance biosensor advanced by long range surface plasmons and magnetic nanoparticle assays. *Anal Chem* 84(19):8345–8350. <https://doi.org/10.1021/ac301904x>
- Li BL et al (2016) Low-dimensional transition metal dichalcogenide nanostructures based sensors. *Adv Funct Mater* 26(39):7034–7056. <https://doi.org/10.1002/adfm.201602136>
- Tsai ML et al (2014) Monolayer MoS₂ heterojunction solar cells. *ACS Nano* 8(8):8317–8322. <https://doi.org/10.1021/nn502776h>
- Ouyang Q et al (2016) Sensitivity enhancement of transition metal dichalcogenides/silicon nanostructure-based surface plasmon resonance biosensor. *Sci Rep* 6:1–13. <https://doi.org/10.1038/srep28190>
- Mak KF, Shan J (2016) Photonics and optoelectronics of 2D semiconductor transition metal dichalcogenides. *Nat Photonics* 10(4):216–226. <https://doi.org/10.1038/nphoton.2015.282>
- Wu L et al (2017) Sensitivity enhancement by using few-layer black phosphorus-graphene/TMDCs heterostructure in surface plasmon resonance biochemical sensor. *Sensors Actuators B Chem* 249:542–548. <https://doi.org/10.1016/j.snb.2017.04.110>
- Pandey PS, Raghuwanshi SK, Singh Y (2022) Enhancement of the sensitivity of a surface plasmon resonance sensor using a noble structure based on barium titanate–graphene–silver. *Opt Quantum Electron* 54:417. <https://doi.org/10.1007/s11082-022-03803-8>
- Karki B, Vasudevan B, Uniyal A, Pal A, Srivastava V (2022) Hemoglobin detection in blood samples using a graphene-based surface plasmon resonance biosensor. *Optik (Stuttg)* 270:169947. <https://doi.org/10.1016/j.ijleo.2022.169947>
- Maurya JB, Prajapati YK, Singh V, Saini JP, Tripathi R (2015) Performance of graphene–MoS₂ based surface plasmon resonance sensor using silicon layer. *Opt Quantum Electron* 47(11):3599–3611. <https://doi.org/10.1007/s11082-015-0233-z>
- Rahman MM, Rana MM, Rahman MS, Anower MS, Mollah MA, Paul AK (2020) Sensitivity enhancement of SPR biosensors employing heterostructure of PtSe₂ and 2D materials. *Opt. Mater. (Amst)* 107:110123. <https://doi.org/10.1016/j.optmat.2020.110123>
- Karki B, Uniyal A, Pal A (2022) Advances in surface plasmon resonance – based biosensor technologies for cancer cell detection. *Int J Opt* 2022:1476254. <https://doi.org/10.1155/2022/1476254>
- Panda A, Pukhrambam PD, Keiser G (2020) Performance analysis of graphene-based surface plasmon resonance biosensor for blood glucose and gas detection. *Appl Phys A Mater Sci Process* 126:153. <https://doi.org/10.1007/s00339-020-3328-8>
- Sinha S, Takabayashi Y, Shinohara H, Kitaura R (2016) Simple fabrication of air-stable black phosphorus heterostructures with large-area hBN sheets grown by chemical vapor deposition method. *2D Mater* 3(3):1–6. <https://doi.org/10.1088/2053-1583/3/3/035010>
- Bruna M, Borini S (2009) Optical constants of graphene layers in the visible range. *Appl Phys Lett* 94(3):1–4. <https://doi.org/10.1063/1.3073717>
- Ghosh S, Ray M (2015) Analysis of silicon based surface plasmon resonance sensors with different amino acids. *SILICON* 7(4):313–322. <https://doi.org/10.1007/s12633-015-9293-8>
- Uniyal A, Pal A, Chauhan B (2022) Long-Range SPR sensor employing platinum diselenide and Cytop nanolayers giving improved performance. *Phys B Condens Matter J.* 649:414487. <https://doi.org/10.2139/ssrn.4230023>
- Karki B, Ansari G, Uniyal A, Srivastava V (2022) PtSe₂ and black phosphorus employed for sensitivity improvement in the surface plasmon resonance sensor. *J Comput Electron.* <https://doi.org/10.1007/s10825-022-01975-w>
- Karki B, Uniyal A, Srivastava G, Pal A (2023) Black phosphorus and Cytop nanofilm-based long-range SPR sensor with enhanced quality factor. *J Sensors* 2102915:1–10. <https://doi.org/10.1155/2023/2102915Research>
- Uniyal A et al (2023) Surface plasmon resonance biosensor sensitivity improvement employing of 2D materials and BaTiO₃ with bimetallic layers of silver. *J Mater Sci Mater Electron.* <https://doi.org/10.1007/s10854-023-09821-w>
- Sun P et al (2019) Applied Surface Science Sensitivity enhancement of surface plasmon resonance biosensor based on graphene and barium titanate layers. *Appl Surf Sci* 475:342–347. <https://doi.org/10.1016/j.apsusc.2018.12.283>
- Singh S, Sharma AK, Lohia P, Dwivedi DK, Kumar V, Singh PK (2023) Simulation study of reconfigurable surface plasmon resonance refractive index sensor employing bismuth telluride and MXene nanomaterial for cancer cell detection. *Phys Scr* 98:025813. <https://doi.org/10.1088/1402-4896/acb023>
- Karki B, Ramya KC, Sandhya Devi RS, Srivastava V, Pal A (2022) Titanium dioxide, black phosphorus, and bimetallic layer-based surface plasmon biosensor for formalin detection: numerical analysis. *Opt Quantum Electron* 54(7):11082. <https://doi.org/10.1007/s11082-022-03875-6>

31. Karki B, Uniyal A, Sharma T, Pal A (2022) Indium phosphide and black phosphorus employed surface plasmon resonance sensor for formalin detection : numerical analysis. *Opt Eng* 61(1):017101. <https://doi.org/10.1117/1.OE.61.1.017101>
32. Singh Y, Paswan MK, Raghuwanshi SK (2021) Sensitivity enhancement of SPR sensor with the black phosphorus and graphene with Bi-layer of gold for chemical sensing. *Plasmonics* 16:1781–1790. <https://doi.org/10.1007/s11468-020-01315-3>
33. Sathya N, Karki B, Rane KP, Jha A, Pal A (2022) Tuning and sensitivity improvement of Bi-metallic structure-based surface plasmon resonance biosensor with 2-D ϵ -tin selenide nanosheets. *Plasmonics* 17:1001–1008. <https://doi.org/10.1007/s11468-021-01565-9>
34. Pal A, Jha A (2021) A theoretical analysis on sensitivity improvement of an SPR refractive index sensor with graphene and barium titanate nanosheets. *Optik (Stuttg)* 231:166378. <https://doi.org/10.1016/j.ijleo.2021.166378>
35. Yupapin P, Trabelsi Y, Vigneswaran D, Taya SA, Daher MG, Colak I (2022) Ultra-high-sensitive sensor based on surface plasmon resonance structure having Si and graphene layers for the detection of Chikungunya virus. *Plasmonics* 17(3):1315–1321. <https://doi.org/10.1007/s11468-022-01631-w>

Publisher's Note Springer Nature remains neutral with regard to jurisdictional claims in published maps and institutional affiliations.

Springer Nature or its licensor (e.g. a society or other partner) holds exclusive rights to this article under a publishing agreement with the author(s) or other rightsholder(s); author self-archiving of the accepted manuscript version of this article is solely governed by the terms of such publishing agreement and applicable law.